Supporting Information

<u>Exit-age distribution functions *E(t)* of the microreactors</u>

The dimensionless exit-age distributions *E(t)* recorded at the outlet of the SAR microreactor (Figure S1) show that the axial dispersion model provides an accurate fitting of the output curve at *Re* =6 (0.2 mL/min). Despite the prevailing laminar conditions the flow system based on the SAR microreactor effectively promotes the distribution of tracer in the radial direction. An empty tube with of equivalent ***φ****P-V* would have an approximate length of 1158 mm. For this tube and using the *Sc* of water (~1000) the correlation of the vessel dispersion number of an empty tube provided by Eq. S1 predicts values of $1/Pe_r$ of 0.019, 0.095, 0.191 and 1.90 for the flow rates investigated.

$$\frac{D}{v \cdot d_{eq}} = \frac{1}{\mathrm{Re} \cdot Sc} + \frac{\mathrm{Re} \cdot Sc}{192} \qquad \text{(S1)}$$

At *Re* =6 the vessel dispersion number obtained for the SAR ($1/Pe_r$ ~0.065) is greater than the limit for small deviations from plug flow ($1/Pe_r < 0.01$) and an empty tube with equivalent ***φ****P-V* would yield a narrower distribution at this condition ($1/Pe_r$ ~0.019). At higher *Re* values (Figure S1b-d) the skewness of the output signal shifts to the left of the mean (***d*** =1) exhibiting a sharp first-appearance time followed by a tailing effect, thus the flow system comprising the SAR falls beyond the accuracy of the axial dispersion model for open-open boundary conditions. At those conditions, the distributions exhibit an exponential decay response which is better predicted when a compartment flow model is assumed, *e.g.* a combination of a mixed flow reactor preceded by a plug flow reactor. It is further observed that at *Re* =70 (2.0 mL/min) the *side capacity model* (SCM) provides a better fit of the exponential decay. The SCM physically represents a main mixed flow reactor with constant interchange of fluid with a smaller mixed flow unit connected in parallel. Mixed flow reactors in parallel are used to represent by-passing or stagnancy. Since using both inlets during the experimental runs reduces the risk of stagnant zones, this type or curves support the notion of by-passing already detected in previous sections. By-passing can be produced by an unbalanced flow distribution. Since only flow rate combinations with r_Q =1 are considered in this section, this imbalance is probably caused by the geometry of the SAR manifolds.

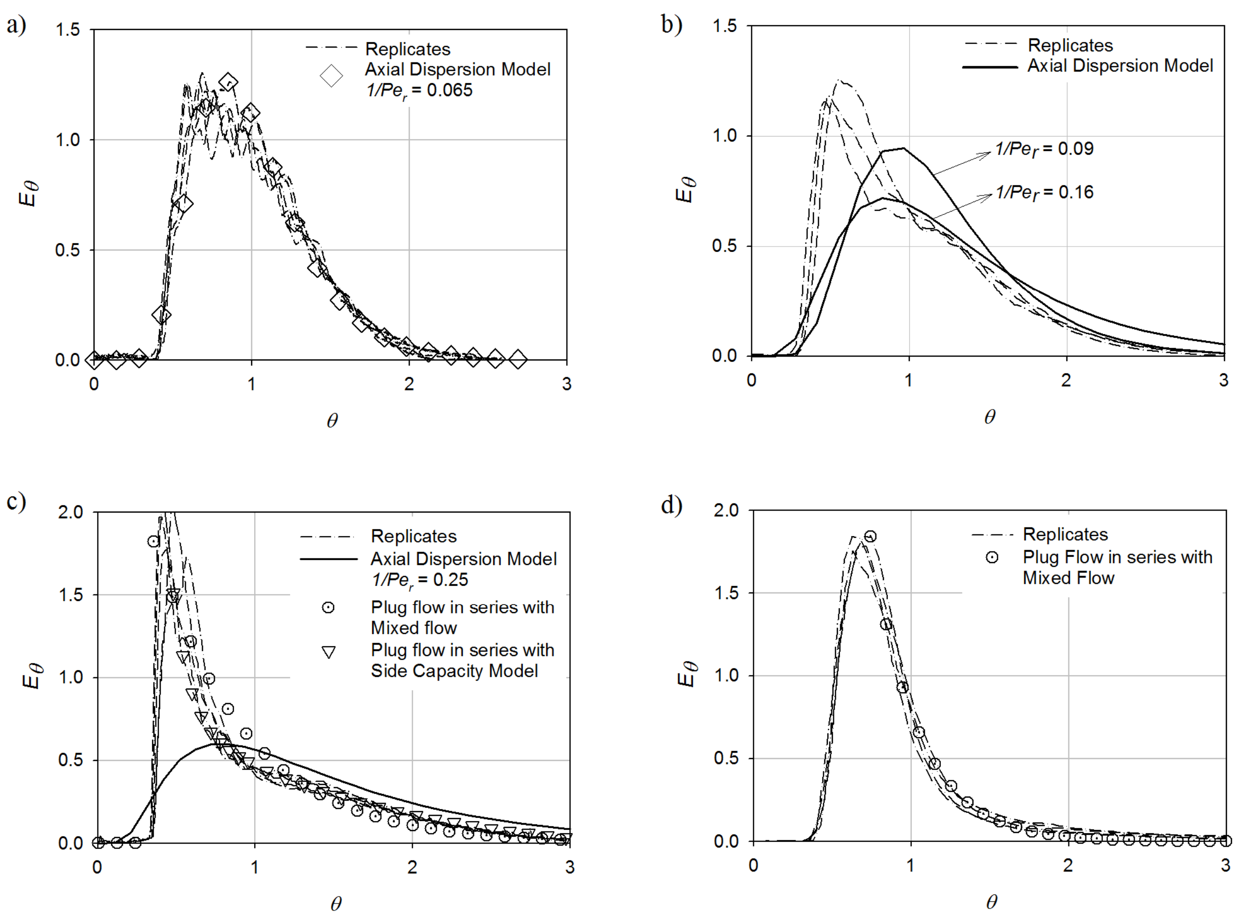

Figure S1. Output signals before deconvolution recorded at the outlet of the SAR microreactor for different *Re*: a) 6 (0.2 mL/min), b) 35 (1.0 mL/min), c) 70 (2.0 mL/min) and d) 665 (20.0 mL/min).

The conclusion from this preliminary analysis of the composite flow system is that from the flow rate range investigated, the most desirable behavior in the SAR microreactor is obtained at *Re* =6 corresponding to a flow rate of 0.2 mL/min (*i.e.* 0.1 mL/min per inlet) where complete mixing in the radial direction is obtained at the longest mean residence time (~170 s) while still achieving a Gaussian distribution. The more Gaussian and narrow a RTD distribution is, the closer the vessel is to plug flow operation. The higher flow conditions exhibit the behavior of vessels with good mixing (*i.e.* mixed flow reactors) although with an exponential distribution. Exponential distributions produce different levels of conversion and in certain chemical reaction applications are not the optimal responses.

A similar qualitative behavior is observed for the LLMR (Figure S2). An empty tube of equivalent $\boldsymbol{\varphi}P\text{-}V$ would have an approximate length of 973 mm. For this tube and using again the *Sc* of water (~1000) the correlation provided by Eq. S1 predicts values of $1/Pe_r$ of 0.023, 0.114, 0.227 and 2.27. This equivalent tube of the LLMR would produce a slightly broader distribution than the equivalent tube of the SAR. However, at *Re* =10 (0.2 mL/min) the actual LLMR microreactor exhibits a narrower RTD ($1/Pe_r$ ~ 0.051) than the SAR microreactor ($1/Pe_r$ ~ 0.065) albeit at the expense of greater pressure drop. Starting at *Re* =52 (1.0 mL/min) the LLMR shows a defined shift towards the mixed flow behavior with the side capacity model providing an accurate fit. Therefore, at higher flow rates (Figure S2c-d) the LLMR flow system cannot be compared directly with the $1/Pe_r$ values predicted by the axial dispersion model for an equivalent circular tube. At *Re* =10 the flow system featuring the LLMR exhibits the behavior of complete radial mixing and a narrow distribution of residence times.

The output curves of both microreactors at *Re* >52 are similar in shape (*e.g.* exponential decay) to those of the input curves recorded at the corresponding flow conditions. The distinctive shapes of the tracer input signals at *Re* <10 are changed to Gaussian distributions after flowing through the microreactors. This improved Gaussian response is attributed to efficient flow distribution and radial homogenization in the complete working volume of the microreactors at sufficiently low fluid velocities. The microfluidic structures are capable to recombine the flow to the extent of improving the non-ideal distribution of the tracer input.

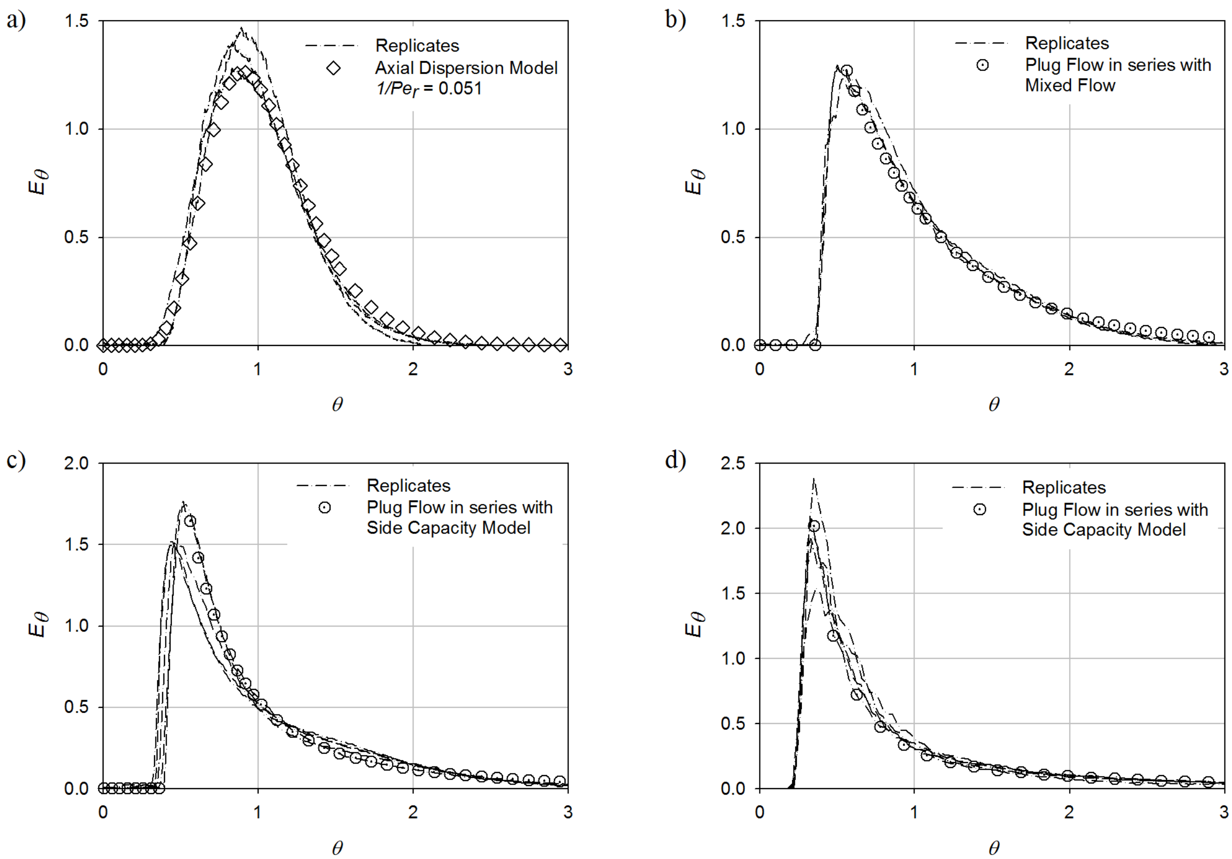

Figure S2. Output signals before deconvolution recorded at the outlet of the LLMR microreactor for different *Re*: a) 10 (0.2 mL/min), b) 52 (1.0 mL/min), c) 105 (2.0 mL/min) and d) 1050 (20.0 mL/min).

Suitability of direct deconvolution in the Fourier domain

To corroborate the validity of the responses obtained by direct deconvolution in the Fourier domain and to verify the accuracy of the axial dispersion model to represent the RTD of the microreactors, the reverse process (*i.e.* convolution in the time domain) was performed. At each flow condition any random replicate of the input was convoluted in the time domain with the fitting curves obtained by the axial dispersion model. The comparison of the calculated signals with any random replicate from the output signals recorded experimentally is shown below.

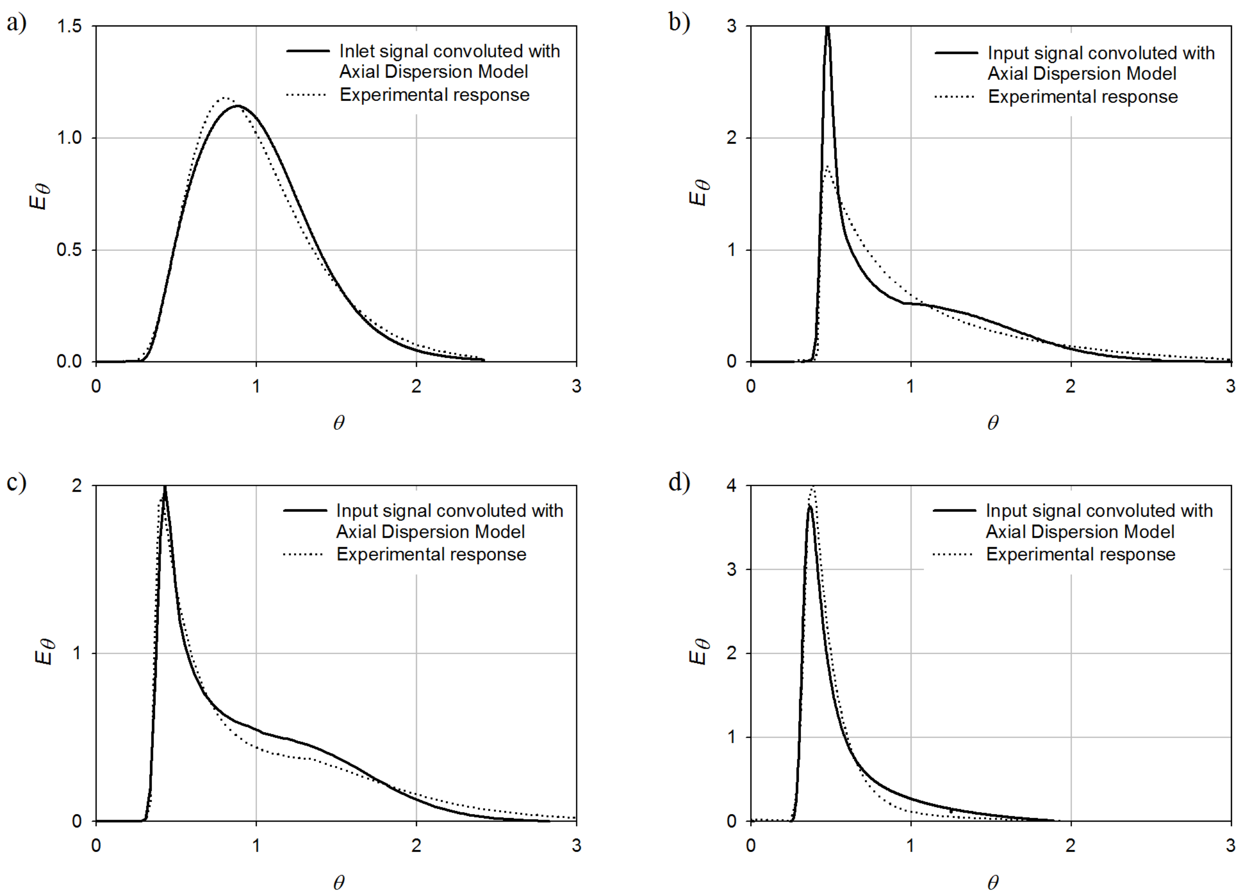

Figure S3. Comparison of the original recorded responses at the outlet of the SAR microreactor with the curves obtained by time domain convolution of the input signals with the axial dispersion model for different *Re*: a) 6, b) 35, c) 70, and d) 665.

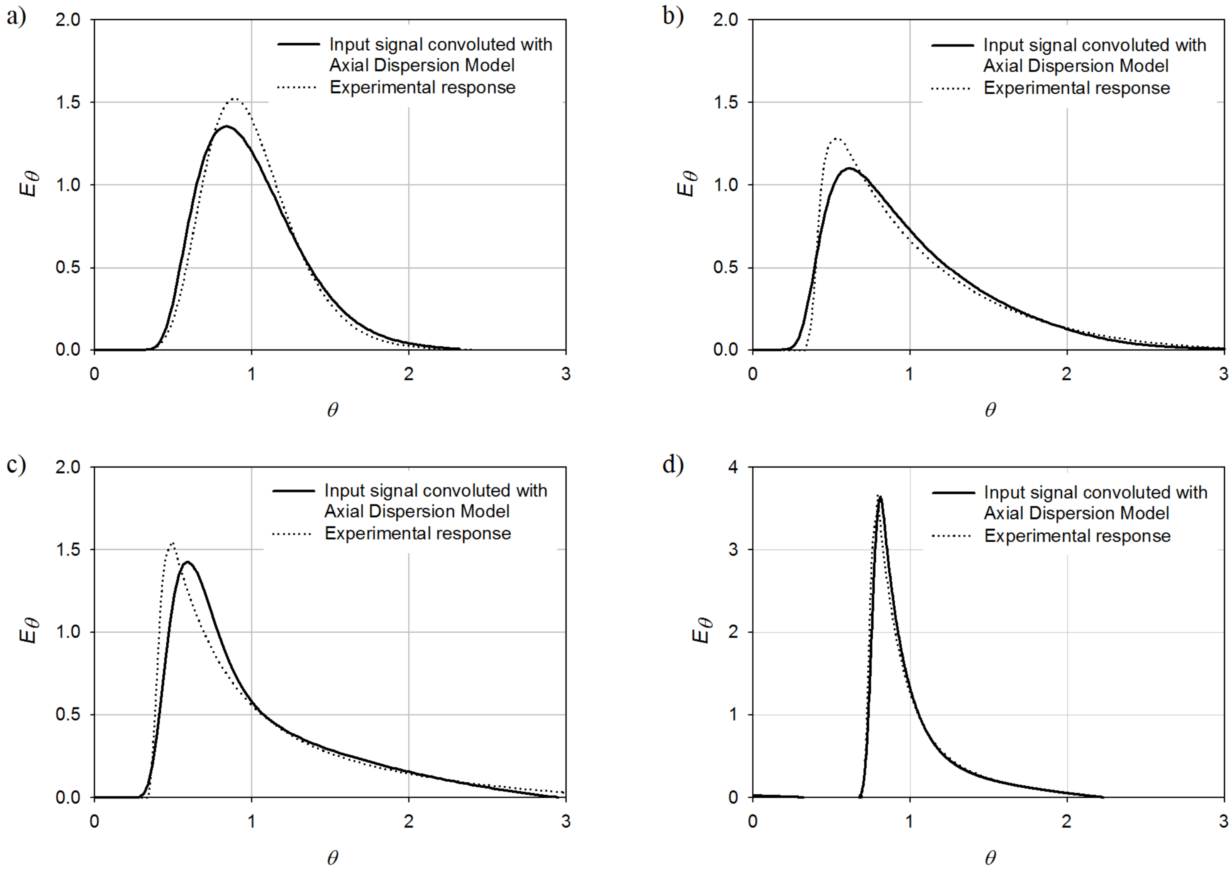

Figure S4. Comparison of the original recorded responses at the outlet of the LLMR microreactor with the curves obtained by time domain convolution of the input signals with the axial dispersion model for different *Re*: a) 10, b) 52, c) 105, d) 1005.